Extended Abstracts of the 2019 International Conference on Solid State Devices and Materials, Nagoya, 2019, pp161-162

On Electronic Structure of Monolayer Tungsten Disulfide Doped by 3*d* Transition Metals

Chieh-Yang Chen[1,2] and Yiming Li[1-3,*]

[1] Parallel and Scientific Computing Laboratory, National Chiao Tung University, Hsinchu 30010, Taiwan
[2] Institute of Communications Engineering, National Chiao Tung University, Hsinchu 30010, Taiwan
[3] Department of Electrical and Computer Engineering, National Chiao Tung University, Hsinchu 30010, Taiwan
*Tel: +886-3-5712121 ext. 52974; Fax: +886-3-5726639; Email: ymli@faculty.nctu.edu.tw

Abstract

In this work, monolayer tungsten disulfide (mWS_2) doped by various 3*d* transition metals (TM), with two different concentrations, 7.13×10^{13} and 2.85×10^{14} cm^{-2}, are studied by density-functional-theory simulation. Not like many studies assuming substitutional doping site, we considered two interstitial (I−) and two substitutional (S−) sites. The work function, the charge transfer, and the projected local density of state are accordingly discussed.

1. Introduction

In recent years, two-dimensional materials The monolayer transition metal dichalcogenide disulfide (TMD) featuring a high on/off ratio, low power consumption, and thermal stability, especially the direct energy band gap of monolayer structure becoming eye-catching study issues. People are seeking methods to adjust the characteristic of TMD materials and the doping issues have recently drawn a lot of attention [1-4]. The value of dopants in monolayer MoS_2 ($mMoS_2$) has been reported [1]; however, many studies focused on the magnetic properties by assuming substitutional doping sites [2-4]. Our recent study revealed the key steps for the stability of doping sites for discussing electronic properties of TMD materials [5-6]. For WS_2, although some doping techniques on monolayer tungsten disulfide (mWS_2) were reported [7-11], they only focused on certain doping material; thus, in this work, we systematically analyzed the doping sites, work function, projected local density of state (PDOS) of mWS_2 with 3*d* transition metals doped mWS_2. Our considered doping materials consist of scandium (Sc), titanium (Ti), vanadium (V), chromium (Cr), manganese (Mn), iron (Fe), cobalt (Co), nickel (Ni), copper (Cu), and zinc (Zn). Two different doping concentrations are 7.13×10^{13} and 2.85×10^{14} cm^{-2} by constructing 4×4 and 2×2 monolayer WS_2 supercell. We use symbols 4×4 and 2×2 as the dimension of the supercell containing a dopant, and the aforementioned effective doping concentrations are 2.04% and 7.69% in the atomic percentage, corresponding to 7.13×10^{13} and 2.85×10^{14} cm^{-2}, respectively.

2. Simulation Methodology

This study uses Vienna ab initio Simulation Package (VASP) [12] to calculate structure relaxation and electronic properties under spin-polarized density functional theory (DFT). Perdew-Burke-Ernzerhof (PBE) is used as an exchange-correlation function since our intensive accuracy test before [5-6]. The cutoff kinetic energy is 500 eV; the force acting on each atom of relaxed structure is smaller than 0.01 eV/Å; the energy difference is less than 10^{-6} per atom. Figure 1 shows verified calculated band structure of (a) bulk and (b) monolayer WS_2. Confidently, the calculated energy bandgaps with different number of layers and bulk material are in agreement with the experiments [13]. To determine the most stable site with lowest formation energy, four possible doping sites are illustrated and discussed, as shown in Fig. 2.

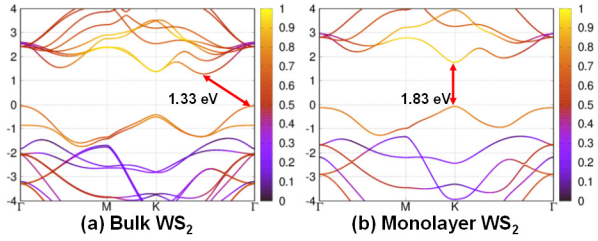

Fig. 1 From simulation, the atom-projected band structure of (a) bulk WS_2 and (b) monolayer WS_2 are obtained. The color bars indicate the weighting of band dominated by tungsten atoms. The indirect bandgap is 1.33 eV and direct bandgap is 1.83 eV for bulk WS_2 and monolayer WS_2, respectively.

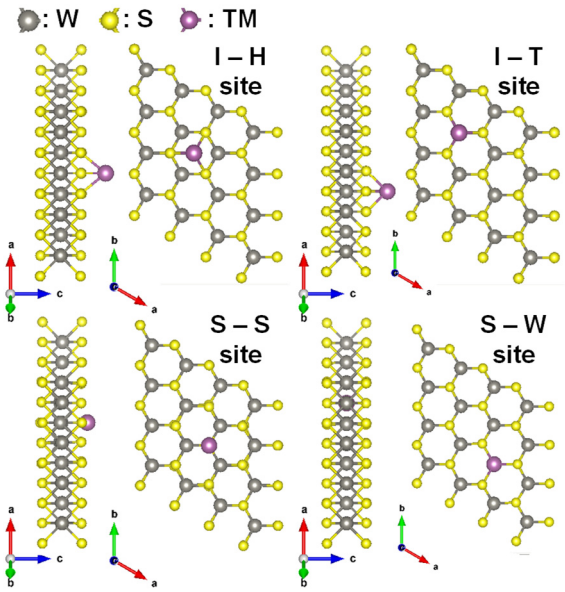

Fig. 2 The structure of four possible doping sites, the gray, yellow, and brown atoms are W, S, and doping transition metal, respectively. Two interstitial (I−) and two substitutional (S−) sites are simulated to determine the most stable site with lowest formation energy.

3. Results and Discussion

One of the interstitial site, I−T, has lowest formation energy for all TM dopant, as listed in Tab. I. The calculated magnetic moments are listed in Tab. II, doping with scandium (Sc) and copper (Cu) results in large change of magnetic moment, about 61.7% and 89% reductions, as doping concentration increases. Figure 3 plots the work function of TM-doped mWS_2 with respect to two concentrations. The titanium (Ti)-doped mWS_2 has the lowest work function while zinc (Zn)-doped has the highest work function. Doping with Sc possesses the largest range of modulation of work function, about 1.63 eV, among different doping species.

Table I The formation energies (eV) of four doping sites for 4×4 mWS_2 supercell.

site	I – H	I – T	S – S	S – W
Sc	-1.735	**-1.855**	1.708	4.806
Ti	-1.656	**-2.245**	1.149	2.620
V	-3.664	**-4.138**	0.302	0.879
Cr	-0.685	**-0.851**	3.673	4.902
Mn	-0.487	**-0.728**	2.986	6.236
Fe	-1.158	**-2.139**	2.336	6.124
Co	-2.170	**-2.713**	2.115	6.667
Ni	-2.670	**-3.202**	1.713	7.722
Cu	-1.051	**-1.092**	3.381	10.177
Zn	-0.033	**-0.036**	5.949	12.437

Table II The total magnetic moments (Mag. Mom.) of doped mono layer WS_2 supercell (SC.) with different doping concentrations.

Mag. Mom.	**Sc**	**Ti**	**V**	**Cr**	**Mn**
4x4 SC.	3	4	5	6	5
2x2 SC.	1.15	4	5	5.62	4.62
Mag. Mom.	**Fe**	**Co**	**Ni**	**Cu**	**Zn**
4x4 SC.	2	1	0	1	0
2x2 SC.	2	1	0	0.11	0

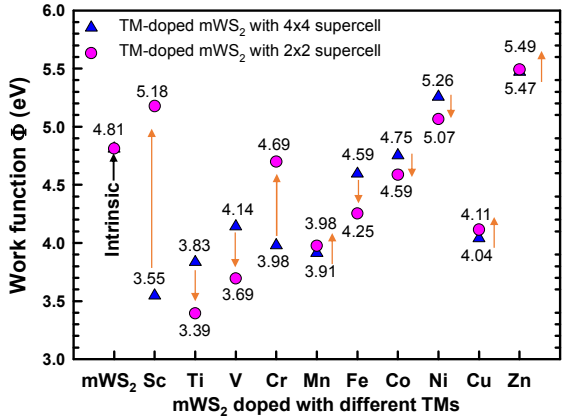

Fig. 3 The work function of TM-doped mWS_2 with respect to different TM materials. The triangle and circle symbols are results of 4×4 and 2×2 supercells, respectively. The most stable structure, I-T, is simulated with two different doping concentrations. The arrows indicate how the work function changes as the doping concentration increases.

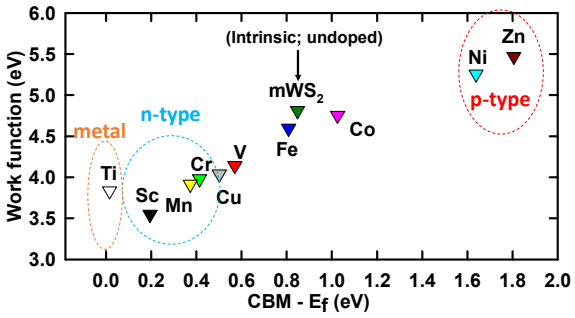

Fig. 4 The work function versus the energy difference between the conduction band minimum (CBM) and the fermi level (E_f) of the TM-doped mWS_2. Ti-doped mWS_2 shows metal behavior; Sc, Mn, and Cr doping can be considered as n-type dopants while Ni and Zn can be used as p-type dopants because the energy differences are much lower and higher than that of intrinsic mWS_2, respectively.

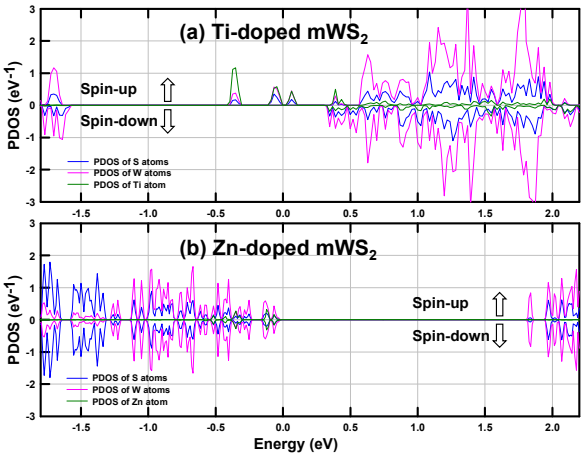

Fig.5: PDOS corresponding to atoms of S, W, and TMs, (a) Ti- and (b) Zn- doped mWS_2, the values of PDOS are normalized to the unit cell of mWS_2.

The difference between conduction band and fermi energy is discussed in Fig. 4. Ti-doped mWS_2 behaves metal; Sc, manganese (Mn), and Chromium (Cr) are suitable for n-type dopant; and nickel (Ni) and Zn are for p-type dopant. Fig.5 shows the PDOS corresponding to atoms of S, W, and TMs. The asymmetric shift of PDOS of spin-up and spin-down indicates the Ti-doped mWS_2 has magnetic properties since Ti dopant contributes the trap-ping energy level close to the fermi level and the contribution of Zn dopant is far from the fermi level.

4. Conclusions

In this work, the electronic and magnetic properties of 3*d* transition metal-doped mWS_2 have been explored. The values of work function of Sc-, Ti-, V-, Cr-, and Fe-doped mWS_2 have relatively large variations, which indicates high flexibility for device design and fabrication. It has been observed that the lowest and highest work function appear at Ti- and Zn-doped mWS_2. The magnetic properties of 3d transition metals: Sc, Cr, Mn, and Cu can be altered by varying doping concentrations.

Acknowledgements

This work was supported in part by the Ministry of Science and Technology, Taiwan, under Grant MOST 106-2221-E-009-149, Grant MOST 106-2622-8-009-013-TM, Grant MOST 107-2622-8-009-011-TM, and Grant MOST 107-2221-E-009-094.

References

[1] X. Lin *et al*., J. Appl. Phys. **116** (2014) 044311.
[2] Y. Wang *et al*., Sci. Rep. **6** (2016) 24153.
[3] C. Huang *et al*., Journal of Semiconductors **38** (2017) 033004.
[4] E. Z. Xu *et al*., Nanoscale **9** (2017) 3576.
[5] Y.-C. Tsai *et al*., IEEE Int. Conf. Simul. Semicond. Process. Devices (SISPAD), pp. 169–172, 2017.
[6] Y.-C. Tsai *et al*., IEEE Trans. Electron Devices **65** (2018) 733.
[7] N. Li *et al*., Solid State Communications, **269** (2018) 58.
[8] S. Sasaki *et al*., Appl. Phys. Express, **9** (2016) 071201.
[9] P. Chen *et al*., Solid State Commun. **230** (2016) 35.
[10] L. Yang *et al*., Nano Lett. **14** (2014) 6275.
[11] C. Sun *et al*., J. Mater. Chem. A **4** (2016) 11234.
[12] G. Kresse *et al*., Phys. Rev. B, Condens. Matter. **47** (1993) 558.
[13] R. Lv *et al*., Acc. Chem. Res. **48** (2015) 56.